HHS Public Access

Author manuscript

J Phys Chem A. Author manuscript; available in PMC 2019 November 21.

Published in final edited form as:

J Phys Chem A. 2018 November 21; 122(46): 9107–9114. doi:10.1021/acs.jpca.8b07163.

Chemical Exchange Reaction Effect on Polarization Transfer Efficiency in SLIC-SABRE

Andrey N. Pravdivtsev[1], **Ivan V. Skovpin**[2,3], **Alexandra I. Svyatova**[2,3], **Nikita V. Chukanov**[2,3], **Larisa M. Kovtunova**[3,4], **Valerii I. Bukhtiyarov**[4], **Eduard Y. Chekmenev**[5,6], **Kirill V. Kovtunov**[2,3], **Igor V. Koptyug**[2,3], and **Jan-Bernd Hövener**[1]

[1]Section for Biomedical Imaging, Molecular Imaging North Competence Center (MOIN CC), Department of Radiology and Neuroradiology, University Medical Center Schleswig-Holstein (UKSH), Kiel University, Am Botanischen Garten 14, 24118 Kiel, Germany

[2]International Tomography Center, SB RAS, Institutskaya st. 3 A, 630090 Novosibirsk, Russia

[3]Novosibirsk State University, Pirogova st. 2, 630090 Novosibirsk, Russia

[4]Boreskov Institute of Catalysis SB RAS, 5 Acad. Lavrentiev Ave., 630090 Novosibirsk, Russia

[5]Department of Chemistry, Wayne State University, Karmanos Cancer Institute (KCI), Integrative Biosciences (Ibio), Detroit, MI 48202, United States

[6]Russian Academy of Sciences, Leninskiy Prospekt 14, 119991 Moscow, Russia

Abstract

Signal Amplification By Reversible Exchange (SABRE) is a new and rapidly developing hyperpolarization technique. The recent discovery of Spin-Lock Induced Crossing SABRE (SLIC-SABRE) shows that high field hyperpolarization transfer techniques developed so far were optimized for singlet spin order that does not coincide with the experimentally produced spin state. Here, we investigate the SLIC-SABRE approach and the most advanced quantitative theoretical SABRE model. It is the goal to achieve the highest possible polarization with SLIC-SABRE at high field using the standard SABRE system, IrIMes catalyst with pyridine. We demonstrate the accuracy of SABRE model describing the effects of various physical parameters such as the amplitude and frequency of the radio-frequency field, and the effects of chemical parameters such as the exchange rate constants. The combined use of experiments and theory allows to determine the effective lifetime of SABRE-complex. Furthermore, the entropy and enthalpy of the SABRE-complex dissociation reaction based on the temperature dependence of SLIC-SABRE signal can be accessed. We show, for the first time, that this SLIC-SABRE model can be useful for the

* **Corresponding Author: Phone:** +49 4318805854, andrey.pravdivtsev@rad.uni-kiel.de.

Author Contributions

The manuscript was written through contributions of all authors. All authors have given approval to the final version of the manuscript

ASSOCIATED CONTENT

Supporting Information

This information is available free of charge via the Internet at http://pubs.acs.org.

Analysis of the average lifetime of SABRE complex, simple SABRE formula, RF-field frequency/amplitude/temperature/k'_d dependences (.avi) and step-by-step description of dissociation rate constant fitting (.PDF).

evaluation of the chemical exchange parameters that are very important for the production of highly polarized contrast agents via SABRE.

Graphical Abstract

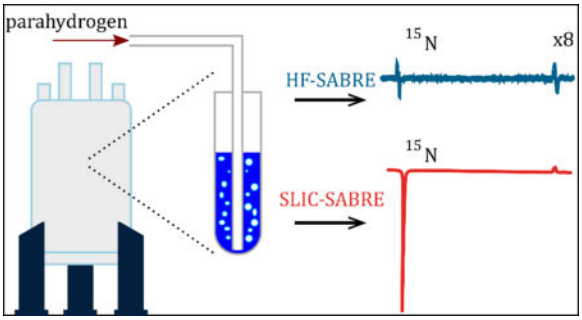

I. Introduction

Nuclear Magnetic Resonance (NMR) is a versatile tool that is extensively applied in science and medicine. Different approaches to increase the sensitivity of the method were proposed during the last decades[1–10]. One of these methods is Signal Amplification By Reversible Exchange[4], SABRE, a ParaHydrogen Induced Polarization (PHIP) technique[11,12], that has shown quite interesting developments[13–24]. SABRE hyperpolarization can be "*spontaneously*" generated at low (mT)[25–28], ultra-low (<μT)[21,29–32] and high (T) magnetic fields[33,34]. High-field SABRE offers an advantage of producing and detecting hyperpolarization at the same location, and therefore, mitigates sample transfer requirements, and offers advantages of signal averaging[35] and permanent addition of pH$_2$[36]. For the high-field regime, several polarization transfer sequences were developed in order to make SABRE more robust and efficient: ^{1}H radio-frequency pulse induced SABRE (^{1}H-RF-SABRE)[37], Low Irradiation Generation of High-Tesla SABRE (LIGHT-SABRE)[38], a method based on the application of adiabatic RF-pulses[39], SABRE-INEPT[40,41], Alternating Delays Achieve Polarization Transfer SABRE (ADAPT-SABRE)[22], SABRE COSY and Sepp-HoSQC[35] and Spin-Lock Induced Crossing SABRE (SLIC-SABRE)[42,43]. SLIC was pioneered by Rosen and co-workers[44]. The sequence has been shown to be very efficient for transformation of nascent *para*hydrogen-derived singlet spin order into observable magnetization[38,45–48].

High-field SABRE not only provides hyperpolarized samples without a need of external polarizers, but allows as well to use all conventional NMR methods to elucidate chemical reaction parameters under fully controlled reaction conditions. For example, even before SABRE was established, modification of INEPT sequence was employed to study the reactivity of different metal-organic complexes[49].

Spin-order transfer (SOT) RF-pulse sequences are typically developed for a specific molecular system. In theory, most of these methods provide a polarization close to the absolute maximum[50]. However, these theoretical values are challenging to reach experimentally. Moreover, the same high-field SOT sequences often provide a much higher

polarization level for systems where pH_2 was added permanently[51] as compared to systems undergoing the reversible exchange[39]. The main reason for this is that the chemical exchange between the catalyst-bound and free states of pH_2 and substrate, S, is continuous, while the duration of a SOT sequence is finite[40]. As a result, only a fraction of all complexes are subjected to the entire SOT sequence. For some pulse sequences, e.g., PH-INEPT[40,41,52], it is crucial that complex does not dissociate during the entire duration of the SOT sequence, otherwise there will be no hyperpolarization.

The substrate polarization in SABRE experiments at high and low fields strongly depends on the experimental conditions: concentration of the catalyst, substrate, pH_2 flow rate, pressure and sample temperature[13,21,40,53–55].

Using a simplified approach to describe the polarization transfer, a “SABRE formula” was introduced[56], encompassing various chemical properties of the SABRE chemical exchange. This model attempts in a simplified manner to explain an effect of chemical exchange on the resulting SABRE polarization level.

Another, more advanced quantitative theory was introduced recently which provides the most accurate theoretical description of SABRE phenomenon to date[53]. This method, however, is restricted to a maximum of 6–7 spins in the SABRE-complex because of computational limitations.

In this work, we investigate the properties of SLIC-SABRE experiments[42], and demonstrate a significant improvement of hyperpolarization level. As it was shown in the original work[42,43], SLIC-SABRE is more tolerant with respect to the initial spin state of the system. At least half of the maximum polarization is retained even when fast S-T_0 mixing occurs. This is different compared to other methods, where the entire signal can be lost (e.g., LIGHT-SABRE[38]). As a result, SLIC-SABRE is a method robustly applicable for a wide range of different metal complexes.

An additional advantage of SLIC-SABRE over other polarization pulse sequences was identified in this work: by fitting a model to experimental SLIC-SABRE data, the effective exchange rate (or mean lifetime) of the SABRE complex can be derived. Only during this time period, polarization transfer occurs before the SABRE complex dissociates[57]. This parameter is critical for achieving high polarization levels. However, as one will find in the Results and discussion section, the current state of the art quantitative SABRE model[53] used in this work does not give a perfect explanation of the experimental results and further improvement of the theory (and experimental protocols) is necessary.

II. Materials and methods

Materials.

All experiments were carried out using a 0.1 M solution of ^{15}N-pyridine (^{15}N-Py) and 5 mM of IrIMes iridium N-heterocyclic carbene complex[13] (IMes = 1,3-bis(2,4,6-trimethylphenyl)imidazole-2-ylidene) in methanol-d_4 (purchased from Carl Roth GmbH, CAS: 811-98-3). ^{15}N-Py and IrIMes were synthesized according to earlier published

procedures[13,58]. The initial IrIMes complex was activated by flushing pH$_2$ through the mixture for 20 minutes, resulting in three molecules of substrate (Py) binding to the complex. The resulting solution consisted of SABRE-active complex [IrH$_2$Imes(Py)$_3$] and free Py, fPy, with 1 to 17 concentration ratio.

Equipment.

pH$_2$ was prepared using commercially available setup with a conversion temperature of 38 K that provides ≈ 90 % enrichment of the para fraction (Bruker, BPHG 90). Experiments were carried out inside a 300 MHz NMR spectrometer (Bruker AVANCE). The reaction chamber for pH$_2$ supply was described before[38]. pH$_2$ is delivered in a standard 5 mm NMR tube (Wilmad) via a thin 1/16” capillary. pH$_2$ flow rate was 7 scm^3/min with 1.7 bar overpressure with respect to an ambient pressure.

Pulse sequences.

We used the previously published SLIC-SABRE pulse sequence[42] with the following modifications (Figure 1): during the acquisition, a ^{1}H WALTZ-16[59] block was added to decouple the pyridine protons to increase SNR and to eliminate an anti-phase spin order. As a result, net polarization of free ^{15}N-pyridine was observed. Hereafter, $^{15}N_{\text{bound}}$ stands for the ^{15}N signal of bound equatorial ^{15}N-Py, and $^{15}N_{\text{free}}$ is for the ^{15}N signal of free ^{15}N-Py. During the experiment, pH$_2$ was constantly supplied by bubbling. No significant distortion of the ^{15}N resonances was observed.

Also, a selective ^{1}H WALTZ-16 decoupling block was added during the continuous wave radio frequency (CW RF) pulse (sequence SLIC/dc-SABRE) to decouple ^{15}N from ^{1}H nuclei of pyridine. The signal of the two hydride protons should not be affected. The decoupling of pyridine protons and ^{15}N significantly simplified the spin system such that the quantitative SABRE theory[53] was used for the simulations of the experiment.

Quantitative SABRE theory.

For a quantitative description of SABRE, the chemical reaction process has to be combined with the spin evolution. The chemical exchange reaction in SABRE can be described with the following set of equations. Association and dissociation of substrate:

$$\mathrm{Ir}H_2S \underset{k_a}{\overset{k_d}{\leftrightarrow}} \mathrm{Ir}H_2 + S \quad \text{(eq1)}$$

Here, $\mathrm{Ir}H_2S$ represents the Ir-complex where H$_2$ and substrate (S) are coordinated and mutual J-couplings exist. $\mathrm{Ir}H_2$ is a transient Ir-complex. k_d and k_a are dissociation and association rate constants, respectively.

Exchange of hydrogen:

$$\mathrm{Ir}H_2 + H_2' \xrightarrow{k_{ex}} \mathrm{Ir}H_2' + H_2 \quad \text{(eq2)}$$

Loss of free hydrogen to exhaust/atmosphere:

$$H_2 \xrightarrow{W_{ex}} exhaust \quad \text{(eq3)}$$

Supply of fresh $p\mathrm{H}_2$ (H_2^*) in solution:

$$supply \xrightarrow{W_{in}} H_2^* \quad \text{(eq4)}$$

The simulation of this set of equations is rather complicated because they are nonlinear. To address this issue, the following simplifications were proposed in the quantitative SABRE theory[53]:

A1.

The reservoir of $p\mathrm{H}_2$ in solution is large: an unlimited amount of $p\mathrm{H}_2$ is always available, at a constant enrichment of 100 %.

A2.

The chemical exchange of H_2 with Ir is fast: H_2 in IrH_2 is always pure $p\mathrm{H}_2$ (we will denote that complex as $\mathrm{Ir}H_2^*$ below).

From these simplifications, the following set of equations follows:

$$\mathrm{Ir}H_2^* + S \xrightarrow{k'_a} \mathrm{Ir}H_2^*S \quad \text{(eq5)}$$

$$\mathrm{Ir}H_2S \xrightarrow{k'_d} \mathrm{Ir}H_2 + S \quad \text{(eq6)}$$

$$\mathrm{Ir}H_2 \xrightarrow{\infty} \mathrm{Ir}H_2^* \quad \text{(eq7)}$$

where the primed association and dissociation rate constants k'_a, k'_d indicate that these are the constants in the simplified models. In general, they are not the same as the constants in the full model (eq 1).

When $p\mathrm{H}_2$ is supplied to the system for a long period of time, a “steady-state” association rate, W_a, can be introduced:

$$W_a = [IrH_2]k'_a = k'_d\frac{[IrH_2S]}{[S]} \quad \text{(eq8)}$$

Since the ratio $[IrH_2S]/[S]$ = complex/substrate is known from the experiment and $W_a = k'_d[IrH_2S]/[S]$, k'_d is the only variable parameter in the model. The meaning of k'_d is the effective dissociation rate constant and $\tau = 1/k'_d$ is the mean lifetime of IrH_2S complex. In the SI we discuss how lifetime of the complex and dissociation constant rate are related as well as the effect of lifetime of the complex on polarization level.

It is expected that polarization level scales linearly with pH$_2$ enrichment, so that polarization level for 90% pH$_2$ differs from that for 100 % pH$_2$ by a factor of about 0.87[23]. The detailed description of how to solve this set of equations was given in the original publication[53]. Here, we used the in-house software to calculate SABRE experiments using this model, where chemical exchange, spin Hamiltonian and relaxation superoperators are implemented and only parameters like T_1-relaxation, chemical shifts, constants of J-coupling and k'_d and W_a need to be specified. A detailed description of the software will be published elsewhere.

Calculation demands.

In this model, relaxation was included using Redfield relaxation theory[60], i.e., using relaxation superoperators that increase computational efforts. We can calculate SABRE complexes for a system with up to 6 spins-½. A single superoperator for a 6 spin-1/2 system is composed of $4^6 \times 4^6 \approx 16777216 \cong 1.7 \times 10^7$ numbers. Adding two more protons would increase the size of the superoperators and hence the complexity of computation by a factor of $4^2 \times 4^2 = 256$; in this case, the calculation of SLIC-SABRE with one set of parameters on a PC with 4.2 GHz processor would require about 180 hours. Consequently, we did not attempt to model the experimental data obtained with SLIC-SABRE (>8 coupled spins-½); instead the SLIC/dc-SABRE data is modeled with the quantitative SABRE theory (4 coupled spins-½).

III. Results and discussion

3.1. SLIC-SABRE: theoretical analysis

In order to determine the optimal conditions for SLIC-SABRE, we calculated the ^{15}N-polarization of the free substrate ($^{15}N_{free}$) as a function of the frequency and amplitude P(ν_{rf}, ν_1) of the CW-pulse.

The computation was performed for a 4-spin-½ SABRE complex [IrH_2S_2], where S was a single ^{15}N nucleus (Figure 2A, simulations details are provided in the caption). P(ν_{rf}, ν_1) was found to be antisymmetric with respect to the frequency of the resonance of a bound substrate, $\nu_{rf} = \nu(^{15}N_{bound})$: two polarization extrema with different signs were observed.

The maximum polarization ≈ 24% was found at ν_1=5 Hz and $\nu_{rf} - \nu(^{15}N_{bound})$=17 Hz (for IrIMes, ^{15}N-Py with decoupled protons in methanol, see J-coupling constants in Table S1).

Similar simulations were already performed in the original SLIC-SABRE work. However, it is important to note that P(ν_{rf}, ν_1) strongly depends on the chosen k'_d (see supplementary video for P(ν_{rf}, ν_1, k'_d) and Figures S4 and S6).

Next, P(k'_d) was simulated for fixed ν_1=5 Hz and $\nu_{rf} - \nu(^{15}N_{bound})$=17 Hz for a 4-spin-½ and 6-spin-½ SABRE complex [IrH_2S_2]. Here, the substrate was assumed to be either a single ^{15}N spin or ^{15}N with ^1H (i.e., a substrate with one ^{15}N nucleus and one ortho-^1H hydrogen of Py). Both systems exhibited a similar P(k'_d) that rises quickly to one maximum and descends slowly to zero. Some of the features are reproduced by the analytical "SABRE formula" from Ref. ([56]) too. The similar peak function was predicted by analytical equation for SABRE at ultra-low magnetic fields (SABRE-SHEATH)[61], however it did not provide satisfactory agreement with the experiments and adaptation for high-field SLIC-SABRE experiment is necessary, therefore we will not use that method and "SABRE formula" in the work.

Although, addition of ^1H to the substrate does not change the shape of P(k'_d), the absolute polarization is reduced by a factor of 2.5. Thus, a reduced spin system appears to be quite beneficial for an increased hyperpolarization yield. Experimentally, we realized that by applying frequency selective ^1H WALTZ-16 decoupling on the Py-protons (see Figure 1, 3, 4 and discussion below). Before, attempts were made to simplify the SABRE system using e.g., substitution of ^1H by ^2H[33,39], however, deuterons also have J-couplings with ^{15}N and often ^2H exchanges with $^1H_2$ in the solution as a result of pH$_2$ bubbling in the presence of an Ir-complex. Unfortunately, we were not able to simulate the system where S = ($^{15}N^1H^1H$), i.e., with both ortho-protons of pyridine taken into account, because of our current computational power limitations.

To summarize, for an optimization of polarization yield, it is required to find the appropriate values of ν_1, ν_{rf} and t_{CW}. Furthermore, the polarization is strongly dependent on k'_d (see supplementary video or Figure 6S), which, in turn, depends on the temperature, the choice of substrate, solvent and catalyst.

3.2. SLIC-SABRE RF-field matching

Using the optimal parameters deduced from simulation, ν_1 = 5 Hz and $\nu_{rf} - \nu(^{15}N_{bound})$=17 Hz, the maximal signal was experimentally observed for a CW duration t_{CW} = 1.17 s. After n=20 repetitions of SLIC, a constant polarization level was achieved. Holding ν_1 = 5 Hz and t_{CW} constant, we varied the frequency offset of the CW RF-pulse, $\nu_{rf} - \nu(^{15}N_{bound})$, at T = 15 °C for both variants of the sequence (Figure 3).

For SLIC/dc-SABRE, the two main extrema at frequencies ±17 Hz and two minor extrema at ±8 Hz were observed. These were well reproduced by the simulations with $k'_d = 14 s^{-1}$.

For SLIC-SABRE, the main extrema were shifted to ±20 Hz and no other extrema were observed.

This experimental data proves that the matching conditions for SLIC-SABRE and SLIC/dc-SABRE are different (because the effective spin systems are different). Note that both ortho-protons effectively contribute and enlarge the spin system in SLIC-SABRE. The polarization is 2.6 times larger in the effectively smaller spin system.

To demonstrate the effect of k'_d, the simulations were repeated with $k'_d = 60\text{s}^{-1}$ (Figure 3). This calculation fails to reproduce experimentally observed SLIC/dc-SABRE data. For more examples of simulated frequency/amplitude/k'_d dependences we refer the reader to Figure S6 (SI) or supplementary video.

3.3. SLIC-SABRE temperature dependence

To investigate the effect of k'_d, we performed experiments at different temperatures with fixed CW RF-field amplitude ν_1 = 5 Hz and frequency offset, $\nu_{rf} - \nu(^{15}N_{\text{bound}})$=17 Hz (SLIC/dc-SABRE) and 20 Hz (SLIC-SABRE) (see Figure 4 and Figure S4 in the **SI**), t_{CW} = 1.17 s and n = 20. The experimental SLIC/dc-SABRE results were simulated using quantitative SABRE theory for a [IrH_2S_2] complex with $S = {}^{15}$N. We also think that it is interesting to mention that temperature variation was used before for optimization of low field ^{1}H-SABRE[54].

To correlate simulated $P(k'_d)$ with experimental P(T), we used conventional Eyring equation in the form $k'_d = \frac{k_B T}{h}\exp\left(\frac{\Delta S^{\ddagger}}{R} - \frac{\Delta H^{\ddagger}}{RT}\right)$ that couples rate constant, k'_d, and temperature, T. A step-by-step procedure of fitting experimental data is given in **SI** (Figure S7).

The same system has been investigated before and data sets for k_d(T) are available, measured with EXSY[13] and SABRE-INEPT[40]. The corresponding entropy, $\Delta S^{\ddagger}$, and enthalpy, $\Delta H^{\ddagger}$, of activation are given in Table 1. Beside EXSY and SABRE-INEPT methods one can use e.g., variation of line-width with temperature to determine the average lifetime of the SABRE complex[61], however, this data for IrIMes with Py are not available and is very hard to obtain, because field homogeneity is disturbed by the bubbling system and a simulation of spectrum of SABRE complex is necessary[61].

Within the error margin the enthalpy, $\Delta H^{\ddagger}$, obtained with SLIC-SABRE method coincides with the results reported in Ref. 40 (SABRE-INEPT). Both SABRE-INEPT and SLIC-SABRE data deviate from the data obtained with EXSY.

Matching the dissociation rate parameters with the previously reported data support the validity of quantitative SABRE theory for describing not only various SABRE polarization transfer methods but also chemical exchange processes responsible for the production of hyperpolarization.

3.4. SLIC-SABRE polarization level

We simulated SLIC/dc-SABRE experiment for various experimental parameters: ν_1, ν_{rf}, t_{CW} and for different values of k'_d (see Figure 2, S6 and supplementary video). The high level of

^{15}N-polarization, ~25 %, was found for the following model parameters: t_{CW} = 1.17 s, n = 20, ν_1=5 Hz,$|\nu_{rf} - \nu(^{15}N_{bound})|$ in the range from 10 Hz to 20 Hz, $k'_d \cong 10 - 30\,s^{-1}$, T_1 relaxation times of IrH_2, ^{15}N in the complex and in the bulk equal to 1 s, 6 s and 60 s respectfully and J-coupling constants given in Table 1S. However, the maximum level of polarization experimentally achieved here with SLIC/dc-SABRE is about 0.45 %, which is far from the theoretical maximum.

We have compared the performance of SLIC-SABRE and LIGHT-SABRE reported in Refs. (38,42,43) with our results (see Table 2S in **SI**). In all cases, the levels of ^{15}N polarization are moderate and fall in the range from 0.0067% to 0.545%. However, for application not only the level of polarization but the total intensity of the polarized signal is very important. To characterize total intensity, we introduce the quantity S which is a product of polarization level (in %) and the concentration of free substrate (in mM). This parameter characterizes the available NMR signal, therefore its value is a measure of efficiency of hyperpolarized agents production.

The achieved values of parameter S are in the range from 0.134 to 45. It is noteworthy that the optimized SLIC-SABRE[43] and the original LIGHT-SABRE[38] experiments give almost the same values (10.9 and 9.7, respectively), while with our optimization and experimental settings the value of 45 was achieved.

The data collected in Table 2S demonstrate clearly that not only the experimental settings used in various studies are different (e.g., duration of some RF pulses) but also the concentration of substrates, catalyst, pH$_2$ pressure and pH$_2$ flow differ as well. SABRE experimental setups are not unified and therefore it is hard to compare the results obtained in different laboratories. However, we are certain that decoupling of substrate protons will always be beneficial for direct and efficient polarization transfer to ^{15}N nuclei in high field SABRE experiments.

At the same time, we note that here the theory is employed for a qualitative estimation of the real system, because several simplifications were used. The main simplification is neglecting the chemical exchange with H_2. Theoretically, one can say that an unlimited supply of pH$_2$ in the bulk is available, however, by SABRE-SHEATH experiment it was perfectly demonstrated that it is not the case: ^{15}N polarization in SABRE-SHEATH experiment increases together with increase of pH$_2$ pressure and a flow rate[21]. Our current theoretical approach is more descriptive of the experimental condition of significantly higher pH$_2$ concentration and gas pressure and therefore, future modifications of the theory are necessary and will be attempted. We believe that including pH$_2$ exchange will be the next step in understanding moderate performance of high field SABRE.

Moreover, the vast majority of modern high-field high-resolution NMR spectrometers have significant experimental and fundamental shortcomings in the context of maximizing the efficiency of SLIC-SABRE. First, and foremost, only a small fraction of the sample is encompassed by the RF coil – as a result, RF pulses often cover only a fraction of the sample. Moreover, the irradiated sample fraction is constantly changing due to continuous pH$_2$ bubbling. Second, significant RF field gradients exist at the ends of the RF coil resulting

in sub-optimal sample irradiation. Third, parahydrogen bubbling creates some susceptibility gradients, which may additionally contribute to lower than expected SLIC pulse efficiency. Last but not least, ^{15}N chemical shift anisotropy decreases the ^{15}N T_1 at high magnetic fields[62], thereby potentially limiting the maximum attainable ^{15}N polarization due to disproportionately greater T_1-associated losses compared to those at lower magnetic fields. Most of these experimental and fundamental limitations can be overcome through the use of lower field magnets (e.g. 1.5 T or lower MRI scanners), which in principle can be equipped with RF coils encompassing the entire SABRE sample with better RF homogeneity and reduced susceptibility induced gradients. Moreover, ^{15}N T_1 times are longer at lower magnetic fields than at higher magnetic fields in the context of SABRE[62]. We also point out that these hardware advances have already been enjoyed by conventional hydrogenative PHIP technique enabling higher polarization values[36,63].

Conclusion

We have analyzed and optimized SLIC-SABRE polarization transfer technique for IrIMes SABRE catalyst with pyridine in methanol. Under optimal conditions we obtained the polarization level of 0.45% for 100 mM Py which corresponds to about 1900-fold enhancement at 7 T. When parameter S which is equal to the product of polarization and concentration is compared, the signal intensity achieved in this work is higher than in the original SLIC-SABRE and LIGHT-SABRE experiments. We have shown that quantitative SABRE model is valid for the description of SABRE experiments at high fields even though for calculations performed on a personal computer the SABRE complex can comprise only up to 6 spins ½, whereas for bigger spin systems more powerful computational facilities are required. Alternatively, one can use a ^{1}H decoupling strategy proposed in this work. Moreover, proton decoupling during the pulse sequence not only simplifies the computation procedure but also increases the level of achievable polarization. Using quantitative SABRE model approach, we have shown that SLIC-SABRE method allows one to determine the effective lifetime of the complexes that varies from 8 ms to 476 ms with temperature variation from 35 °C down to 0 °C, and that is similar to the previously published INEPT-based analysis[40]. When one determines an effective lifetime of the complex, the quantitative model can be used to predict the most appropriate low or high field conditions for any SABRE polarization transfer procedure. However, for evaluation of kinetic parameters the use of conventional EXSY experiments may still be more reliable. We believe that this work is important in the context that current elaborate SABRE theory give a hint but does not quantitatively reproduce experimental results, and further improvement of the theory is necessary.

Supplementary Material

Refer to Web version on PubMed Central for supplementary material.

ACKNOWLEDGMENT

A.P. and J.-B.H. acknowledge support by the Emmy Noether Program of the DFG (HO 4604/2–1). Kiel University and the Medical Faculty are acknowledged for supporting the Molecular Imaging North Competence Center (MOIN CC) as core facility for imaging *in vivo*. MOIN CC was founded by a grant of the European Regional

Development Fund (ERDF) and the Zukunftsprogramm Wirtschaft of Schleswig-Holstein (Project no. 122-09-053). E.Y.C. thanks the following for funding: NSF CHE-1416268 and 1836308, NIH 1R21EB020323 and 1R21CA220137, DOD CDMRP W81XWH-12-1-0159/BC112431. IVK and IVS thank Federal Agency for Scientific Organizations (#0333-2017-0002) for support of the parahydrogen activation studies. KVK, AIS, NVC and LMK thank the grant from the Russian Science Foundation (17-73-20030) for the support of SABRE catalyst synthesis and its testing with pyridine.

REFERENCES

(1). Kaptein R Chemically Induced Dynamic Nuclear Polarization in Five Alkyl Radicals. Chem. Phys. Lett 1968, 2 (4), 261–267.

(2). Eisenschmid TC; Kirss RU; Deutsch PP; Hommeltoft SI; Eisenberg R; Bargon J; Lawler RG; Balch AL Para Hydrogen Induced Polarization in Hydrogenation Reactions. J. Am. Chem. Soc 1987, 109 (26), 8089–8091.

(3). Maly T; Debelouchina GT; Bajaj VS; Hu K-N; Joo C-G; Mak–Jurkauskas ML; Sirigiri JR; van der Wel PCA; Herzfeld J; Temkin RJ; et al. Dynamic Nuclear Polarization at High Magnetic Fields. J. Chem. Phys 2008, 128 (5), 052211. [PubMed: 18266416]

(4). Adams RW; Aguilar JA; Atkinson KD; Cowley MJ; Elliott PIP; Duckett SB; Green GGR; Khazal IG; López-Serrano J; Williamson DC Reversible Interactions with Para-Hydrogen Enhance NMR Sensitivity by Polarization Transfer. Science 2009, 323 (5922), 1708–1711. [PubMed: 19325111]

(5). Griesinger C; Bennati M; Vieth HM; Luchinat C; Parigi G; Höfer P; Engelke F; Glaser SJ; Denysenkov V; Prisner TF Dynamic Nuclear Polarization at High Magnetic Fields in Liquids. Prog. Nucl. Magn. Reson. Spectrosc 2012, 64, 4–28. [PubMed: 22578315]

(6). Hirsch ML; Kalechofsky N; Belzer A; Rosay M; Kempf JG Brute-Force Hyperpolarization for NMR and MRI. J. Am. Chem. Soc 2015, 137 (26), 8428–8434. [PubMed: 26098752]

(7). Khurana D; Mahesh TS Bang-Bang Optimal Control of Large Spin Systems: Enhancement of $^{13}C–^{13}C$ Singlet-Order at Natural Abundance. J. Magn. Reson 2017, 284, 8–14. [PubMed: 28938135]

(8). Buckenmaier K; Rudolph M; Back C; Misztal T; Bommerich U; Fehling P; Koelle D; Kleiner R; Mayer HA; Scheffler K; et al. SQUID-Based Detection of Ultra-Low-Field Multinuclear NMR of Substances Hyperpolarized Using Signal Amplification by Reversible Exchange. Sci. Rep 2017, 7 (1), 13431. [PubMed: 29044168]

(9). Nelson SJ; Kurhanewicz J; Vigneron DB; Larson PEZ; Harzstark AL; Ferrone M; van Criekinge M; Chang JW; Bok R; Park I; et al. Metabolic Imaging of Patients with Prostate Cancer Using Hyperpolarized [1-^{13}C]Pyruvate. Sci. Transl. Med 2013, 5 (198), 198ra108–198ra108.

(10). Cunningham CH; Lau JY; Chen AP; Geraghty BJ; Perks WJ; Roifman I; Wright GA; Connelly KA Hyperpolarized 13C Metabolic MRI of the Human Heart: Initial Experience. Circ. Res 2016, CIRCRESAHA.116.309769.

(11). Bowers CR; Weitekamp DP Transformation of Symmetrization Order to Nuclear-Spin Magnetization by Chemical Reaction and Nuclear Magnetic Resonance. Phys. Rev. Lett 1986, 57 (21), 2645–2648. [PubMed: 10033824]

(12). Bowers CR; Weitekamp DP Parahydrogen and Synthesis Allow Dramatically Enhanced Nuclear Alignment. J. Am. Chem. Soc 1987, 109 (18), 5541–5542.

(13). Cowley MJ; Adams RW; Atkinson KD; Cockett MCR; Duckett SB; Green GGR; Lohman JAB; Kerssebaum R; Kilgour D; Mewis RE Iridium N-Heterocyclic Carbene Complexes as Efficient Catalysts for Magnetization Transfer from Para-Hydrogen. J. Am. Chem. Soc 2011, 133 (16), 6134–6137. [PubMed: 21469642]

(14). Glöggler S; Colell J; Appelt S Para-Hydrogen Perspectives in Hyperpolarized NMR. J. Magn. Reson 2013, 235, 130–142. [PubMed: 23932399]

(15). Franzoni MB; Buljubasich L; Spiess HW; Münnemann K Long-Lived ^{1}H Singlet Spin States Originating from Para-Hydrogen in Cs-Symmetric Molecules Stored for Minutes in High Magnetic Fields. J. Am. Chem. Soc 2012, 134 (25), 10393–10396. [PubMed: 22690781]

(16). Pravdivtsev AN; Yurkovskaya AV; Vieth H-M; Ivanov KL; Kaptein R Level Anti-Crossings Are a Key Factor for Understanding Para-Hydrogen-Induced Hyperpolarization in SABRE Experiments. ChemPhysChem 2013, 14 (14), 3327–3331. [PubMed: 23959909]

(17). Eshuis N; van Weerdenburg BJA; Feiters MC; Rutjes FPJT; Wijmenga SS; Tessari M Quantitative Trace Analysis of Complex Mixtures Using SABRE Hyperpolarization. Angew. Chem. Int. Ed 2015, 54 (5), 1481–1484.

(18). Theis T; Ortiz GX; Logan AWJ; Claytor KE; Feng Y; Huhn WP; Blum V; Malcolmson SJ; Chekmenev EY; Wang Q; et al. Direct and Cost-Efficient Hyperpolarization of Long-Lived Nuclear Spin States on Universal $^{15}N_2$-Diazirine Molecular Tags. Sci. Adv 2016, 2 (3), e1501438. [PubMed: 27051867]

(19). Kovtunov KV; Kovtunova LM; Gemeinhardt ME; Bukhtiyarov AV; Gesiorski J; Bukhtiyarov VI; Chekmenev EY; Koptyug IV; Goodson BM Heterogeneous Microtesla SABRE Enhancement of ^{15}N NMR Signals. Angew. Chem. Int. Ed 2017, 56 (35), 10433–10437.

(20). Schmidt AB; Berner S; Schimpf W; Müller C; Lickert T; Schwaderlapp N; Knecht S; Skinner JG; Dost A; Rovedo P; et al. Liquid-State Carbon-13 Hyperpolarization Generated in an MRI System for Fast Imaging. Nat. Commun 2017, 8, ncomms14535.

(21). Truong ML; Theis T; Coffey AM; Shchepin RV; Waddell KW; Shi F; Goodson BM; Warren WS; Chekmenev EY 15N Hyperpolarization by Reversible Exchange Using SABRE-SHEATH. J. Phys. Chem. C 2015, 119 (16), 8786–8797.

(22). Roy SS; Stevanato G; Rayner PJ; Duckett SB Direct Enhancement of Nitrogen-15 Targets at High-Field by Fast ADAPT-SABRE. J. Magn. Reson 2017, 285, 55–60. [PubMed: 29102821]

(23). Hovener J-B; Pravdivtsev AN; Kidd B; Bowers CR; Glöggler S; Kovtunov KV; Plaumann M; Katz-Brull R; Buckenmaier K; Jerschow A; et al. Parahydrogen-Based Hyperpolarization for Biomedicine. Angew. Chem. Int. Ed 2018, 57, 11140.

(24). Kovtunov KV; Pokochueva E; Salnikov O; Cousin S; Kurzbach D; Vuichoud B; Jannin S; Chekmenev E; Goodson B; Barskiy D; et al. Hyperpolarized NMR: D-DNP, PHIP, and SABRE. Chem. Asian J 2018, 13, 1857.

(25). Dücker EB; Kuhn LT; Münnemann K; Griesinger C Similarity of SABRE Field Dependence in Chemically Different Substrates. J. Magn. Reson 2012, 214, 159–165. [PubMed: 22153915]

(26). Hövener J-B; Schwaderlapp N; Lickert T; Duckett SB; Mewis RE; Highton LAR; Kenny SM; Green GGR; Leibfritz D; Korvink JG; et al. A Hyperpolarized Equilibrium for Magnetic Resonance. Nat. Commun 2013, 4, ncomms3946.

(27). Pravdivtsev AN; Ivanov KL; Yurkovskaya AV; Petrov PA; Limbach H-H; Kaptein R; Vieth H-M Spin Polarization Transfer Mechanisms of SABRE: A Magnetic Field Dependent Study. J. Magn. Reson 2015, 261, 73–82. [PubMed: 26529205]

(28). Hövener J-B; Schwaderlapp N; Borowiak R; Lickert T; Duckett SB; Mewis RE; Adams RW; Burns MJ; Highton LAR; Green GGR; et al. Toward Biocompatible Nuclear Hyperpolarization Using Signal Amplification by Reversible Exchange: Quantitative in Situ Spectroscopy and High-Field Imaging. Anal. Chem 2014, 86 (3), 1767–1774. [PubMed: 24397559]

(29). Barskiy DA; Shchepin RV; Coffey AM; Theis T; Warren WS; Goodson BM; Chekmenev EY Over 20% 15N Hyperpolarization in Under One Minute for Metronidazole, an Antibiotic and Hypoxia Probe. J. Am. Chem. Soc 2016, 138 (26), 8080–8083. [PubMed: 27321159]

(30). Shchepin RV; Goodson BM; Theis T; Warren WS; Chekmenev EY Toward Hyperpolarized 19F Molecular Imaging via Reversible Exchange with Parahydrogen. ChemPhysChem 2017, 18 (15), 1961–1965. [PubMed: 28557156]

(31). Barskiy DA; Shchepin RV; Tanner CPN; Colell JFP; Goodson BM; Theis T; Warren WS; Chekmenev EY The Absence of Quadrupolar Nuclei Facilitates Efficient 13C Hyperpolarization via Reversible Exchange with Parahydrogen. ChemPhysChem 2017, 18 (12), 1493–1498. [PubMed: 28517362]

(32). Kiryutin AS; Yurkovskaya AV; Zimmermann H; Vieth H-M; Ivanov KL Complete Magnetic Field Dependence of SABRE-Derived Polarization. Magn. Reson. Chem 2017, 56, 651–662.

(33). Barskiy DA; Kovtunov KV; Koptyug IV; He P; Groome KA; Best QA; Shi F; Goodson BM; Shchepin RV; Coffey AM; et al. The Feasibility of Formation and Kinetics of NMR Signal Amplification by Reversible Exchange (SABRE) at High Magnetic Field (9.4 T). J. Am. Chem. Soc 2014, 136 (9), 3322–3325. [PubMed: 24528143]

(34). Pravdivtsev AN; Yurkovskaya AV; Petrov PA; Vieth H-M; Ivanov KL Analysis of the SABRE (Signal Amplification by Reversible Exchange) Effect at High Magnetic Fields. Appl. Magn. Reson 2016, 47 (7), 711–725.

(35). Hermkens NKJ; Aspers RLEG; Feiters MC; Rutjes FPJT; Tessari M Trace Analysis in Water-Alcohol Mixtures by Continuous p-H_2 Hyperpolarization at High Magnetic Field. Magn. Reson. Chem 2018, 56, 633–640. [PubMed: 29220098]

(36). Schmidt AB; Berner S; Braig M; Zimmermann M; Hennig J; von Elverfeldt D; Hövener J-B In Vivo 13C-MRI Using SAMBADENA. PLOS ONE 2018, 13 (7), e0200141. [PubMed: 30001327]

(37). Pravdivtsev AN; Yurkovskaya AV; Vieth H-M; Ivanov KL RF-SABRE: A Way to Continuous Spin Hyperpolarization at High Magnetic Fields. J. Phys. Chem. B 2015, 119 (43), 13619–13629. [PubMed: 25970807]

(38). Theis T; Truong M; Coffey AM; Chekmenev EY; Warren WS LIGHT-SABRE Enables Efficient in-Magnet Catalytic Hyperpolarization. J. Magn. Reson 2014, 248, 23–26. [PubMed: 25299767]

(39). Pravdivtsev AN; Yurkovskaya AV; Zimmermann H; Vieth H-M; Ivanov KL Transfer of SABRE-Derived Hyperpolarization to Spin-1/2 Heteronuclei. RSC Adv 2015, 5 (78), 63615–63623.

(40). Pravdivtsev AN; Yurkovskaya AV; Zimmermann H; Vieth H-M; Ivanov KL Enhancing NMR of Insensitive Nuclei by Transfer of SABRE Spin Hyperpolarization. Chem. Phys. Lett 2016, 661, 77–82.

(41). Knecht S; Kiryutin AS; Yurkovskaya AV; Ivanov KL Re-Polarization of Nuclear Spins Using Selective SABRE-INEPT. J. Magn. Reson 2018, 287, 10–14. [PubMed: 29274936]

(42). Knecht S; Kiryutin AS; Yurkovskaya AV; Ivanov KL Efficient Conversion of Anti-Phase Spin Order of Protons into 15N Magnetization Using SLIC-SABRE. arXiv 2018.

(43). Knecht S; Kiryutin AS; Yurkovskaya AV; Ivanov KL Efficient Conversion of Anti-Phase Spin Order of Protons into ^{15}N Magnetisation Using SLIC-SABRE. Mol. Phys 2018, (DOI: 10.1080/00268976.2018.1515999).

(44). DeVience SJ; Walsworth RL; Rosen MS Preparation of Nuclear Spin Singlet States Using Spin-Lock Induced Crossing. Phys. Rev. Lett 2013, 111 (17), 173002. [PubMed: 24206484]

(45). Kovtunov KV; Truong ML; Barskiy DA; Koptyug IV; Coffey AM; Waddell KW; Chekmenev EY Long-Lived Spin States for Low-Field Hyperpolarized Gas MRI. Chem. Eur. J 2014, 20 (45), 14629–14632. [PubMed: 25263795]

(46). Kovtunov KV; Truong ML; Barskiy DA; Salnikov OG; Bukhtiyarov VI; Coffey AM; Waddell KW; Koptyug IV; Chekmenev EY Propane-D6 Heterogeneously Hyperpolarized by Parahydrogen. J. Phys. Chem. C 2014, 118 (48), 28234–28243.

(47). Barskiy DA; Salnikov OG; Shchepin RV; Feldman MA; Coffey AM; Kovtunov KV; Koptyug IV; Chekmenev EY NMR SLIC Sensing of Hydrogenation Reactions Using Parahydrogen in Low Magnetic Fields. J. Phys. Chem. C 2016, 120 (51), 29098–29106.

(48). Barskiy DA; Salnikov OG; Romanov AS; Feldman MA; Coffey AM; Kovtunov KV; Koptyug IV; Chekmenev EY NMR Spin-Lock Induced Crossing (SLIC) Dispersion and Long-Lived Spin States of Gaseous Propane at Low Magnetic Field (0.05T). J. Magn. Reson 2017, 276, 78–85. [PubMed: 28152435]

(49). Atkinson KD; Cowley MJ; Duckett SB; Elliott PIP; Green GGR; López-Serrano J; Khazal IG; Whitwood AC Para-Hydrogen Induced Polarization without Incorporation of Para-Hydrogen into the Analyte. Inorg. Chem 2009, 48 (2), 663–670. [PubMed: 19072592]

(50). Goldman M; Jóhannesson H Conversion of a Proton Pair Para Order into 13C Polarization by Rf Irradiation, for Use in MRI. C. R. Phys 2005, 6 (4), 575–581.

(51). Pravdivtsev AN; Yurkovskaya AV; Lukzen NN; Ivanov KL; Vieth H-M Highly Efficient Polarization of Spin-1/2 Insensitive NMR Nuclei by Adiabatic Passage through Level Anticrossings. J. Phys. Chem. Lett 2014, 5 (19), 3421–3426. [PubMed: 26278456]

(52). Bär S; Lange T; Leibfritz D; Hennig J; von Elverfeldt D; Hövener J-B On the Spin Order Transfer from Parahydrogen to Another Nucleus. J. Magn. Reson 2012, 225, 25–35. [PubMed: 23103392]

(53). Knecht S; Pravdivtsev AN; Hövener J-B; Yurkovskaya AV; Ivanov KL Quantitative Description of the SABRE Process: Rigorous Consideration of Spin Dynamics and Chemical Exchange. RSC Adv 2016, 6 (29), 24470–24477.

(54). Zeng H; Xu J; Gillen J; McMahon MT; Artemov D; Tyburn J-M; Lohman JAB; Mewis RE; Atkinson KD; Green GGR; et al. Optimization of SABRE for Polarization of the Tuberculosis Drugs Pyrazinamide and Isoniazid. J. Magn. Reson 2013, 237, 73–78. [PubMed: 24140625]

(55). Appleby KM; Mewis RE; Olaru AM; Green GGR; Fairlamb IJS; Duckett SB Investigating Pyridazine and Phthalazine Exchange in a Series of Iridium Complexes in Order to Define Their Role in the Catalytic Transfer of Magnetisation from Para-Hydrogen. Chem. Sci 2015, 6 (7), 3981–3993. [PubMed: 29218168]

(56). A. Barskiy D; N. Pravdivtsev A; L. Ivanov K; V. Kovtunov K; V. Koptyug I A Simple Analytical Model for Signal Amplification by Reversible Exchange (SABRE) Process. Phys. Chem. Chem. Phys 2016, 18 (1), 89–93. [PubMed: 26645782]

(57). Hövener J-B; Knecht S; Schwaderlapp N; Hennig J; von Elverfeldt D. Continuous Re-Hyperpolarization of Nuclear Spins Using Parahydrogen: Theory and Experiment. ChemPhysChem 2014, 15 (12), 2451–2457. [PubMed: 25079961]

(58). Whaley TW; Ott DG Syntheses with Stable Isotopes: Pyridine-^{15}N. J. Label. Compd 10 (2), 283–286.

(59). Shaka AJ; Keeler J; Frenkiel T; Freeman R An Improved Sequence for Broadband Decoupling: WALTZ-16. Journal of Magnetic Resonance (1969) 1983, 52 (2), 335–338.

(60). Kowalewski J; Mäler L Nuclear Spin Relaxation in Liquids: Theory, Experiments, and Applications; Chemical Physics; Taylor&Francis, 2006.

(61). Colell JFP; Logan AWJ; Zhou Z; Shchepin RV; Barskiy DA; Ortiz GX; Wang Q; Malcolmson SJ; Chekmenev EY; Warren WS; et al. Generalizing, Extending, and Maximizing Nitrogen-15 Hyperpolarization Induced by Parahydrogen in Reversible Exchange. J. Phys. Chem. C 2017, 121 (12), 6626–6634.

(62). Shchepin RV; Jaigirdar L; Chekmenev EY Spin–Lattice Relaxation of Hyperpolarized Metronidazole in Signal Amplification by Reversible Exchange in Micro-Tesla Fields. J. Phys. Chem. C 2018, 122 (9), 4984–4996.

(63). Waddell KW; Coffey AM; Chekmenev EY In Situ Detection of PHIP at 48 MT: Demonstration Using a Centrally Controlled Polarizer. J. Am. Chem. Soc 2011, 133 (1), 97–101. [PubMed: 21141960]

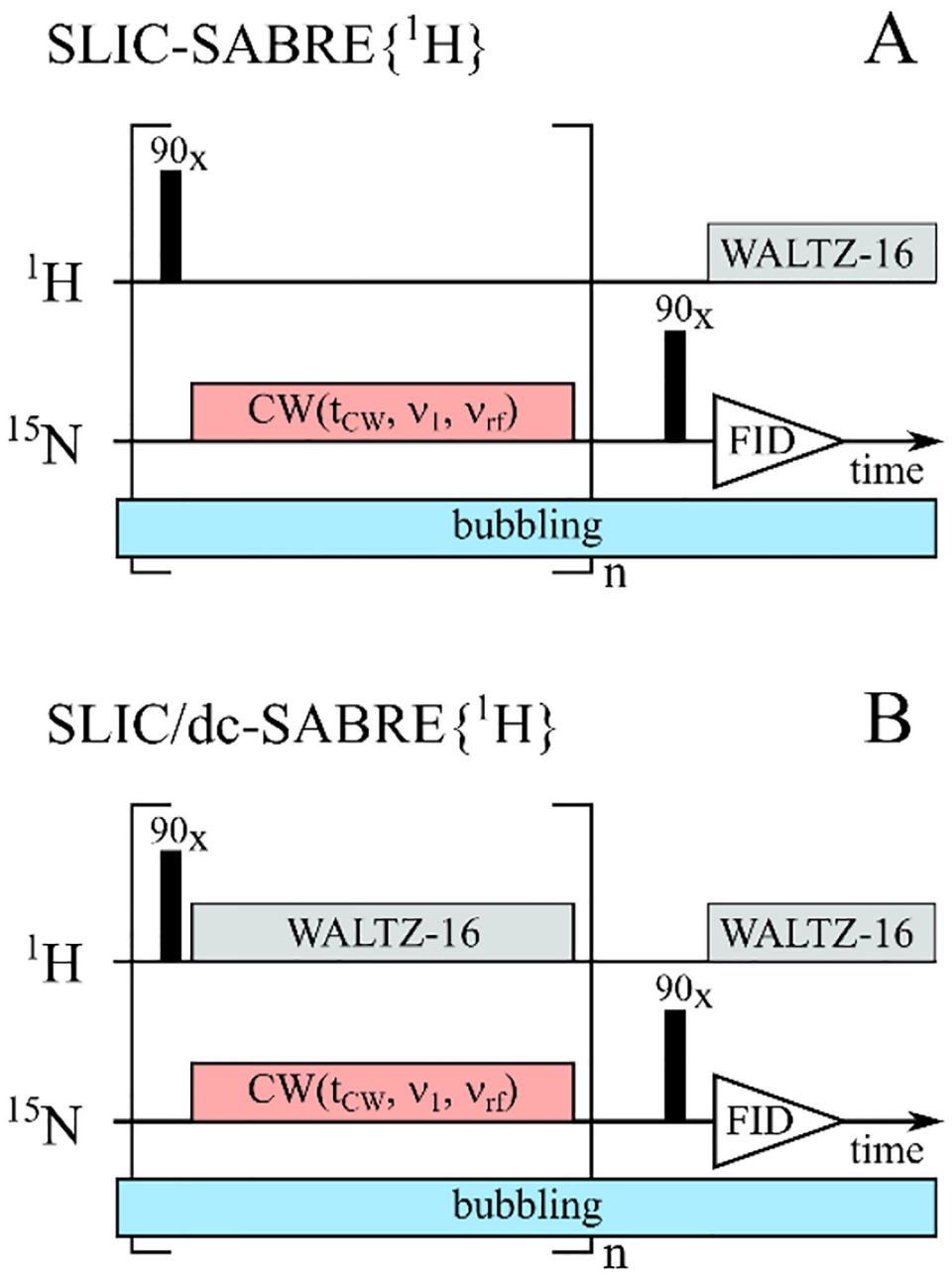

Figure 1.

Schematic view of the original SLIC-SABRE{^{1}H} (A) and modified SLIC/dc-SABRE{^{1}H} (B) sequences, without and with ^{1}H-decoupling during pH$_2$ bubbling, respectively. Typical parameters of the CW field were ν_1 = 5 Hz, $\nu_{rf} \cong$ 255.5 ppm with duration t_{CW} = 1.17 s, the amplitude of WALTZ-16 decoupling block was 300 Hz and carrier frequency was set at 8.3 ppm, durations of 90^o ^{1}H and ^{15}N RF-pulses were 26.7 μs and 21 μs, respectively. The SLIC block in brackets was repeated n = 20 times.

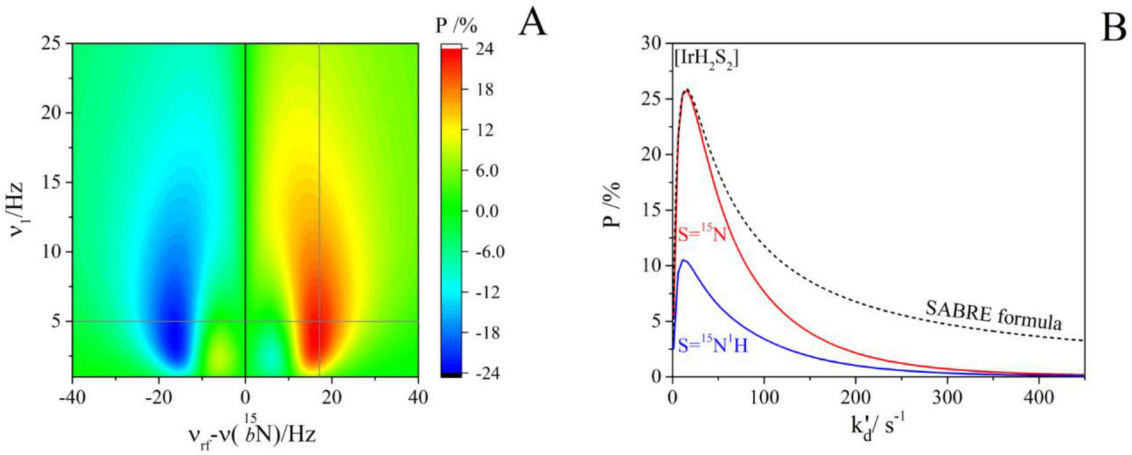

Figure 2.

(A) Simulated $^{15}N_{free}$ polarization as a function of CW RF field amplitude, ν_1, and frequency offset from $^{15}N_{bound}$ resonance, $\nu_{rf} - \nu(^{15}N_{bound})$ for a $[IrH_2S_2]$ SABRE complex, where S = ^{15}N. Note that two distinct extrema occur, symmetric with respect to the frequency of the bound substrate, $\nu(^{15}N_{bound})$. The maximum polarization for $k'_d = 30\ s^{-1}$, $W_a = k'_d/17$, $t_{CW} = 1.17$ s and n = 20 occurs at ν_1=5 Hz and $\nu_{rf} - \nu(^{15}N_{bound})$=17 Hz. (B) Polarization of SLIC-SABRE as a function of k'_d for an $[IrH_2S_2]$ complex with S=^{1}H (red) and S=$^{15}N^{1}H$ (blue) and the “simple analytical SABRE formula” (dashed line).

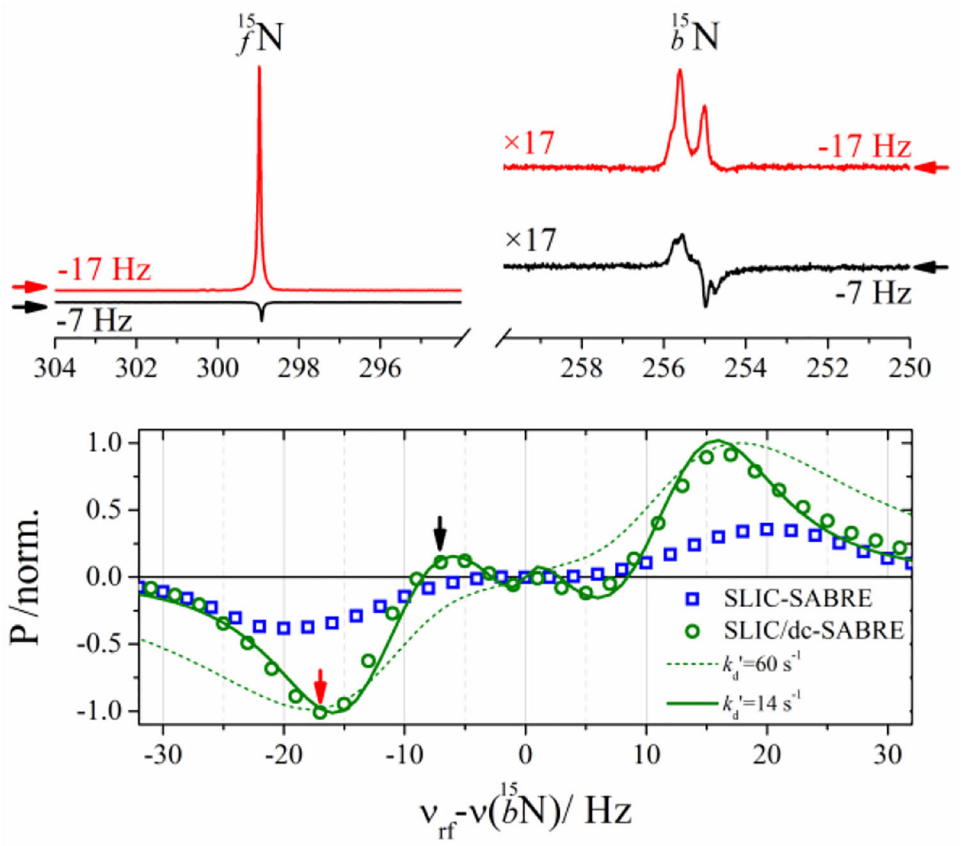

Figure 3.

(Top) High-resolution ^{15}N NMR spectra of free ($^{15}N_{free}$) and bound ($^{15}N_{bound}$) ^{15}N-Py signals after application of SLIC/dc-SABRE{^{1}H} with v_1 = 5 Hz, n=20 and v_{rf} − $v(^{15}N_{bound})$=−17 Hz (red) or −7 (black) at T = 15 °C,. (Bottom) Normalized polarization level of SLIC/dc-SABRE{^{1}H} (green circles) and SLIC-SABRE{^{1}H} (blue squares) as a function of v_{rf} − $v(^{15}N_{bound})$. Green lines are the result of quantitative SABRE model for [IrH_2S_2] complex with $S = {}^{15}N$ and $k'_d = 14\ s^{-1}$ (solid line) or 60 s^{-1} (dashed line). Arrows indicate the offsets corresponding to the spectra demonstrated above.

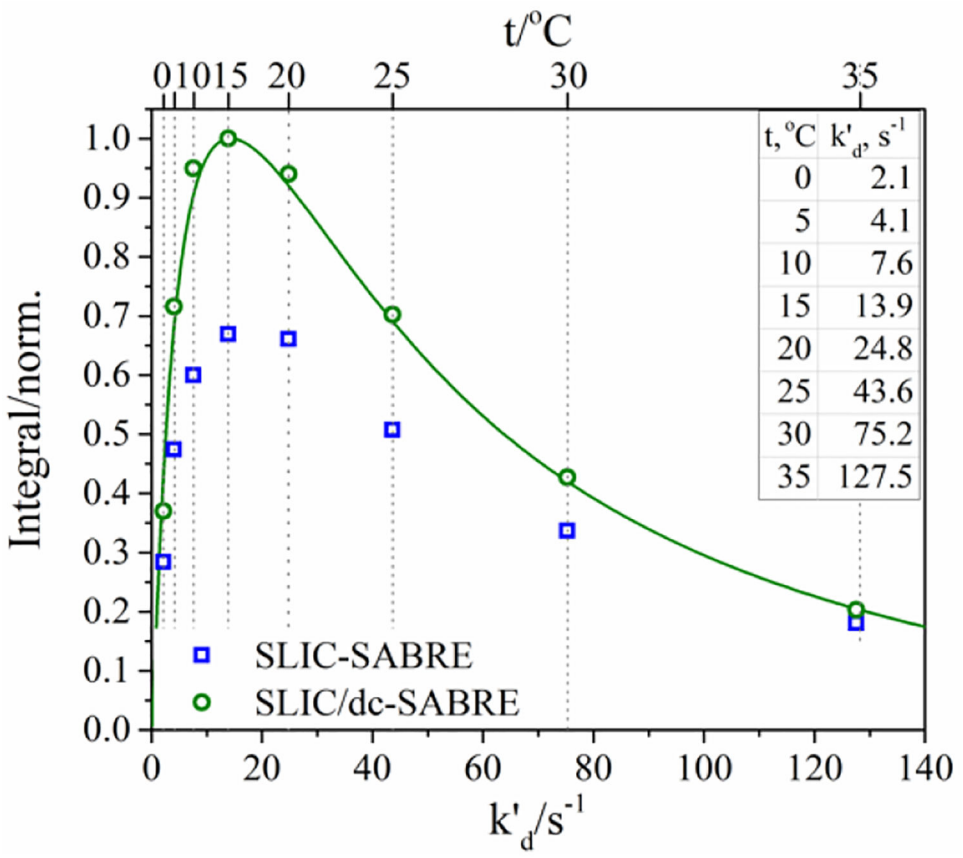

Figure 4.

Experimentally measured SLIC-SABRE{^{1}H} (blue squares) and SLIC/dc-SABRE{^{1}H} (green circles) signal amplitudes as a function of temperature and effective dissociation constant rate, k'_d. Corresponding quantitative SABRE theory simulations (solid lines) for a $[IrH_2S_2]$ complex with S=^{15}N. To interrelate temperature and dissociation rate, Eyring equation with entropy $\Delta S^{\ddagger}$ = 52.9 J/mol·K and enthalpy $\Delta H^{\ddagger}$ = 79.4 kJ/mol of activation was used.

Table 1.

Entropy, $\Delta S^{\ddagger}$, and enthalpy, $\Delta H^{\ddagger}$, of activation for dissociation of pyridine from SABRE complex obtained by fitting EXSY[13], SABRE-INEPT[40] and SLIC/dc-SABRE (this work) temperature dependences of the dissociation rate constant.

	$\Delta S^{\ddagger}$, J/mol·K	$\Delta H^{\ddagger}$, kJ/mol
Ref. 13	97±9	93±3
Ref. 40	33.3±4	76.2±3
this work	52.9±14	79.4±4